Publication II

Y. Hancock, J. Suorsa, E. Tölö, and A. Harju. 2008. Fractional periodicity and magnetism of extended quantum rings. Physical Review B, volume 77, number 15, 155103, 9 pages.

Fractional periodicity and magnetism of extended quantum rings

Y. Hancock,[1,*] J. Suorsa,[1] E. Tölö,[1,2] and A. Harju[1,2]
[1]*Laboratory of Physics, Helsinki University of Technology, P.O. Box 4100, FI-02015 HUT, Finland*
[2]*Helsinki Institute of Physics, University of Helsinki, P.O. Box 64, FI-00014 Helsinki, Finland*

(Received 23 November 2007; revised manuscript received 10 January 2008; published 2 April 2008)

The magnetic properties and nature of the persistent current in small flux-penetrated t-t'-U rings are investigated. An effective rigid-rotator description is formulated for this system, which coincides with a transition to a ferromagnetic state in the model. The criteria for the onset of effective rigid rotation is given. The model is used to understand continuum model ground-state solutions for a two-dimensional few-particle hard-wall quantum dot, where ferromagnetic solutions are found even without the Zeeman coupling to spin. After the onset of an effective rigid rotation, a 97%–98% correspondence can be determined between the lattice model and continuum model eigenstate results.

DOI: 10.1103/PhysRevB.77.155103 PACS number(s): 71.10.Fd, 73.23.Ra, 73.21.La, 74.25.Ha

I. INTRODUCTION

Electron traps in semiconductor materials[1] are nanosystems that are of intense current interest. Examples include quantum rings and dots, which, due to their atomlike features, have shown immense potential for technological application. Recently, it has been a goal to acquire a more fundamental understanding of these systems. For quantum rings, this interest has been partly motivated by the experimental observation of Aharonov–Bohm oscillations and persistent currents.[2,3] In the strictly one-dimensional (1D) limit, the quantum ring can be studied by applying both a discrete model, such as the Hubbard model,[4] and continuum model approaches. In the strongly interacting limit, a correspondence is found between these two sets of results—the electrons become localized and the spin state of the system becomes that of the antiferromagnetic Heisenberg Hamiltonian.[5,6] Electron localization causes the system to become a "rigid rotator." In this case, only the rotational degree of freedom exists so that a change in the magnetic flux results in a change in the angular momentum state of the ring.

The fractional periodicity seen in the Hubbard model and continuum model solutions has been well documented.[7–10] Physical insight into these properties can be obtained from the ground-state energy Bethe Ansatz results for the 1D Hubbard chain with magnetic flux.[7] The ground-state energy as a function of flux Φ consists of a sequence of parabolic segments having Φ_o/N_e periodicity. Here $\Phi_o=h/e$ is the flux quantum and N_e is the number of electrons. In the strongly interacting limit, the ground-state solution at a given value of the flux can be obtained by creating a single hole in the magnon sea. As the flux is increased, the hole is found to move from one Fermi point to the next. The $U\rightarrow\infty$ Bethe Ansatz solutions of the Hubbard model show that the energy has a $(M-N_e\frac{\Phi}{\Phi_0})^2$ flux dependence.[6] The energy minima are found at $\Phi/\Phi_o=M/N_e$, where M is the angular momentum.[11] The minima of the parabolas and fractional periodicity are related to the change in angular momentum state as the flux is increased through the ring. In the $U\rightarrow\infty$ limit, the ground-state Bethe Ansatz solution becomes that of the antiferromagnetic Heisenberg chain,[7] thereby justifying both the rigid-rotator description and antiferromagnetism seen in the continuum model results.[5]

The present work explores the fractional periodicity in flux-penetrated t-t'-U ring systems. The t-t'-U lattice model is a Hubbard model with an additional next-nearest-neighbor hopping t' term.[12] For any 1D system with nearest-neighbor hopping, the ground state is unmagnetized when there is a real and particle-symmetric density-dependent interaction.[13] Thus, these criteria are met for the single-band Hubbard model, but not for the t-t'-U system due to the particle-hole symmetry breaking t' term.[12] In the latter case, no definite order is enforced to the particles, and thus, the possibility of a ferromagnetic state arises. Studies on the 1D t-t'-U chain have indeed verified an extensive ferromagnetic phase for this system.[12] Although much work has been done to understand the t-t'-U model, little is understood about the t-t'-U flux-penetrated ring. Recent investigations of the kinetic t-t' ($U=0$) system with magnetic-flux penetration have indicated an order of magnitude increase in the persistent current due to the addition of the next-nearest-neighbor hopping term.[14] To date, no investigations of the role of interaction effects in flux-penetrated extended-hopping systems have been made.

The physics of the flux-penetrated t-t'-U ring will be shown to explain the continuum model solutions for a circularly symmetric 2D hard-wall quantum dot. In the quantum dot, the strong electron-electron interactions confine the electrons to a ringlike geometry of finite width. The continuum model solution for the flux-penetrated system is shown to have ferromagnetic correlations, with fractional periodicity in the ground-state energy as a function of the penetrating flux. The ferromagnetism seen in this system is in contrast to the antiferromagnetic ground-state result obtained in the limit of the purely 1D ring. The t-t'-U model, which is considered to be the minimal model for ferromagnetism, is therefore thought to be an appropriate choice for probing the ferromagnetic behaviour seen in the continuum model results. By comparing the lattice model and the continuum model solutions, criteria can then be established for obtaining a correspondence between these two sets of results. These criteria can then be used to obtain a microscopic understanding of the ferromagnetism in the dot, as well as to explain the fractional periodicity in the ground-state energy results.

The paper is organized as follows. Section II describes the lattice model and theoretical method. This is followed by

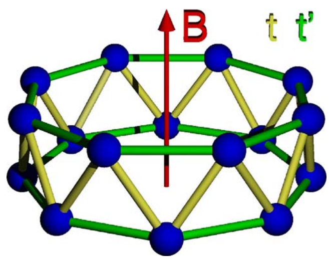

FIG. 1. (Color online) Geometry of the t-t'-U ring with penetrating magnetic flux. In accordance with Ref. 12, the combination of the nearest- and next-nearest-neighbor hopping terms is shown to distort the 1D geometry, resulting in a system consisting two coupled 1D chains. To illustrate this feature, the two rings are displaced along the direction of the magnetic field. This is done for visualization purposes only and does not alter the physics of the model.

Sec. III, the results and discussion, which is divided into two parts. Part A of Sec. III details the quarter-filled flux-penetrated t-t'-U ring system. The flux-penetrated Hubbard model is first discussed as this provides an appropriate context by which to understand the flux-penetrated t-t'-U results. Specific criteria are then established to explain the onset of fractional periodicity seen in the t-t'-U ring as a function of t'/t and U/t. Part B of Sec. III shows an application of the physics of the flux-penetrated t-t'-U ring by determining the correspondence between this and the continuum model results for a few-particle 2D hard-wall quantum dot. The criteria for this correspondence are given together with a discussion of the underlying physical mechanisms, which lead to these results. Section IV concludes the main findings of this work.

II. LATTICE MODEL AND THEORETICAL METHOD

The Hamiltonian for the single-band flux-penetrated t-t'-U ring is

$$H = - t\sum_{i\sigma} (c^{\dagger}_{i+1\sigma}c_{i\sigma}e^{-i\phi} + \text{H.c.}) - t'\sum_{i\sigma} (c^{\dagger}_{i+2\sigma}c_{i\sigma}e^{-2i\phi} + \text{H.c.}) + \sum_i U_i n_{i\uparrow}n_{i\downarrow}. \tag{1}$$

Here, $c^{\dagger}_{i\sigma}(c_{i\sigma})$ creates (destroys) an electron with spin $\sigma=\{\uparrow,\downarrow\}$ at site i in the system, and $n_{i\sigma}=c^{\dagger}_{i\sigma}c_{i\sigma}$ is the number operator. The parameters t and t' are nearest and next-nearest neighbor hopping terms, respectively. The L-site ring system is penetrated by magnetic flux Φ, which is encapsulated in the hopping part of the Hamiltonian, such that

$$\phi = \frac{2\pi}{L}\frac{\Phi}{\Phi_0}. \tag{2}$$

The interaction term is the local Coulomb interaction between opposite spins, the Hubbard U. All parameters are specified in arbitrary units of energy and relative to the nearest-neighbor hopping parameter t. Figure 1 shows the geometry of the t-t'-U ring with flux penetration. Note how the t'/t interaction distorts the chain and introduces a quasi-two-dimensional aspect to the model.

The basis functions for the lattice model are defined using an occupation number basis,

$$|\psi_\alpha\rangle = |n_{\alpha 1\uparrow}\cdots n_{\alpha N\uparrow};n_{\alpha 1\downarrow}\cdots n_{\alpha N\downarrow}\rangle. \tag{3}$$

The ground-state eigenstate $|\Psi\rangle_{\text{lattice}}$ is then a linear combination of these basis functions,

$$|\Psi\rangle_{\text{lattice}} = \sum_{\alpha=1}^{\text{HS}} a_\alpha|\psi_\alpha\rangle, \tag{4}$$

where a_α are the coefficients of the basis states and $\text{HS}=\binom{L}{N_{e\uparrow}}\binom{L}{N_{e\downarrow}}$ is the size of the Hilbert space. Here, $N_{e\uparrow}$ and $N_{e\downarrow}$ refer to the number of spin-up and spin-down electrons, respectively. As only small system sizes are considered, the eigenproblem remains computationally tractable and can be solved by exact diagonalization using the ARPACK solver.[15] The ground-state energy E_0 and persistent current I are investigated as a function of Φ, where

$$I(\Phi) = -\frac{\partial E_0(\Phi)}{\partial \Phi}. \tag{5}$$

To determine the magnetic state of the system, the total spin S is calculated. The local moment, $\langle S_i^2\rangle=\frac{3}{4}\langle m_i^2\rangle$, is used to measure the degree of spin localization. For a quarter-filled chain, the local moment has a maximum value of $\frac{3}{8}$.

III. RESULTS AND DISCUSSION

A. Properties of the flux-penetrated t-t'-U chain as a function of U/t and t'/t

Before discussing the physics of the flux-penetrated t-t'-U ring, it will be necessary to review the flux-penetrated Hubbard chain as this will provide an important base comparison for the t-t'-U extended model. In Fig. 2(a), the ground-state energy as a function of the flux is shown for an eight-site Hubbard ring at quarter filling. The results are for three different interaction strengths, $U/t=20$, 200, and 1000. The periodicity in the ground-state energy is found to change from Φ_o to Φ_o/N_e as the interaction strength is increased to large values and approaches perfect fractional periodicity as $U\rightarrow\infty$. At large interaction strengths, e.g., at $U/t=1000$, the angular momentum values at the minimum of the parabolas follow the expected $\Phi/\Phi_o=M/N_e$ relation. Thus, the $M=0$, 1, 2, 3, and 4 angular momentum states, for example, correspond to $\Phi/\Phi_o=0$, 0.25, 0.5, 0.75, and 1.0, respectively.

In Fig. 2(b), the persistent current is shown for the $U/t=1000$ Hubbard ring. The change in positive to negative current corresponds to the minima of the parabolas in Fig. 2(a). The jump from a minimum to a maximum current is indicative of the change in the angular momentum state of this system. The amplitude of the persistent current is seen to be almost constant as a function of the penetrating flux. This near-perfect fractional periodicity corresponds to the system being an "effective rigid rotator." At $U=\infty$, perfect fractional periodicity and, hence, full rigid rotation would occur. In this case, the amplitude of the persistent current would be constant.

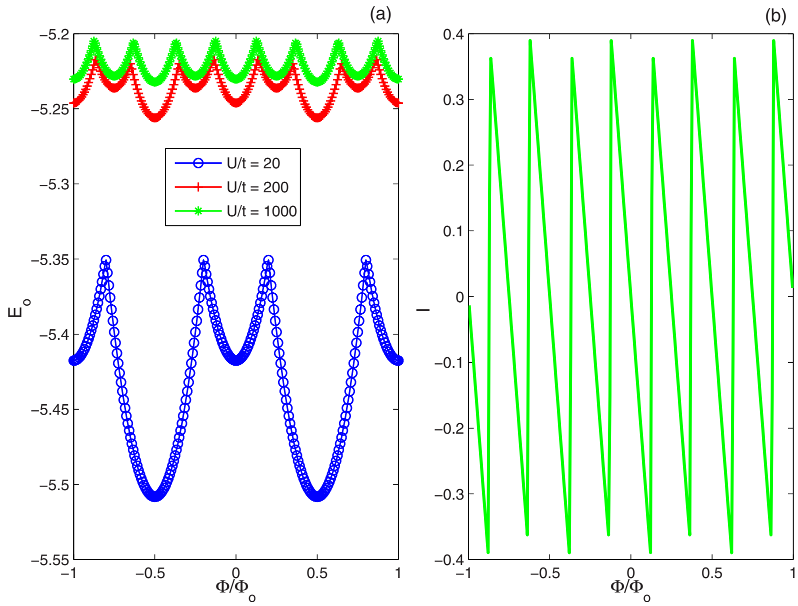

FIG. 2. (Color online) (a) Ground-state energy as a function of flux for an eight-site Hubbard system at quarter filling (2↑, 2↓), $U/t=20$, $U/t=200$ and 1000. (b) Persistent current as a function of flux for the $U/t=1000$ result.

Figure 3 shows the ground-state energy for the quarter-filled t-t'-U system as a function of flux, with $U/t=8$ and $t'/t=-0.05$. The application of the small t'/t term is found to induce marked differences in the ground-state energy as a function of the flux strength, thus demonstrating the sensitivity of the solutions to a small t'/t perturbation. An interesting deviation from the Hubbard results occurs—namely, an early onset of the fractional periodicity with respect to U/t. This effect is clearly evidenced in Fig. 3(b) by the appearance of the $\Phi/\Phi_o=\pm 0.25$ parabolas in the $U/t=20$ result. At $U/t\sim 40.2$, the t-t'-U system becomes an effective rigid rotator, which can be seen in the near-perfect fractional periodicity of the $U/t=40.2$ solution. In comparison, for the Hubbard ring, larger values of the Hubbard U (i.e., $U/t\geqslant 1000$) were required in order to achieve this effect. The Hubbard results show that the fractional periodicity improves as a function of increasing Hubbard U strength. In the t-t'-U system, however, the fractional periodicity acquires its optimal state at moderate values of the Hubbard U. Increasing U/t for the t-t'-U system destroys the near-perfect fractional periodicity due to the "freezing" of the energetics in the $\Phi/\Phi_o=\pm 0.5$ result as a function of increasing U/t. In this case, the energy corresponding to the ground-state solution at $\Phi/\Phi_o=\pm 0.5$ remains the same for $U/t\geqslant 40.2$.

Inspection of the total spin as a function of U/t at $\Phi/\Phi_o=\pm 0.5$ shows that the system has undergone a magnetic transition at $U/t\sim 40.2$ from a $S=0$ to a $S=2$ fully polarized ferromagnetic spin state. The ferromagnetic transition can be confirmed by comparing the energies corresponding to the lowest energy $S=0$ and $S=2$ spin states at $\Phi/\Phi_o=\pm 0.5$, as a function of increasing U/t. At $U/t=20$, the ground state has $S=0$ with an energy gap of 0.12 to the next state, which is $S=2$. At $U/t\sim 40.2$, the lowest energy $S=0$ and $S=2$ spin states are nearly degenerate—the $S=2$

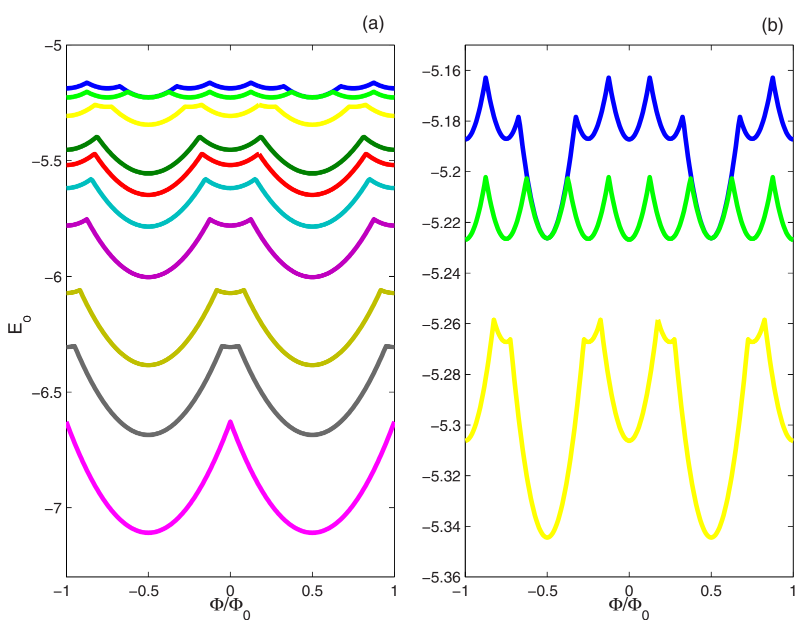

FIG. 3. (Color online) (a) Ground-state energy as a function of flux for an eight-site t-t'-U system at quarterfilling (2↑, 2↓), with $t'/t=-0.05$. The values of U/t starting from the bottom curve are 0, 1, 2, 4, 6, 8, 10, 20, 40.2, and 1000. $U/t=40.2$ is specifically shown as this indicates the onset of effective rigid rotation and, hence, near-perfect fractional periodicity. (b) Ground-state energy as a function of flux, with focus on the $U/t=20$, 40.2, and 1000 results.

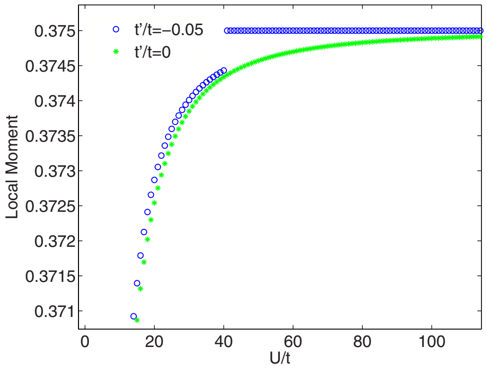

FIG. 4. (Color online) (a) The local moment $\langle S_i^2 \rangle$ as a function of U/t for an eight-site t-t'-U system at quarter filling, $(2\uparrow, 2\downarrow)$. The two solutions are the $\Phi/\Phi_o=0.5$, $t'/t=0$ and $t'/t=-0.05$ results, as indicated in the legend. Note the discontinuity in the $t'/t=-0.05$ solution, which occurs at the onset of effective rigid rotation ($U/t \simeq 40.2$) and corresponds to the $S=0 \to 2$ ferromagnetic transition.

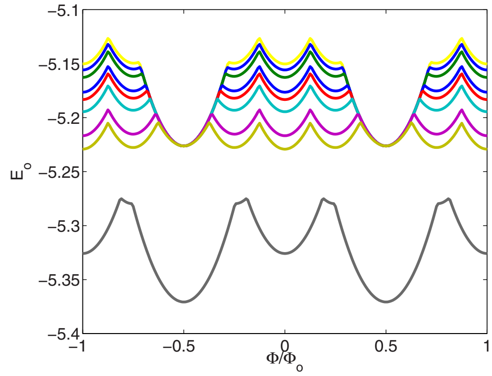

FIG. 5. (Color online) (a) Ground-state energy as a function of flux for an eight-site t-t'-U system at quarter filling, $(2\uparrow, 2\downarrow)$, with $t'/t=-0.1$. The values of U/t starting from the bottom curve are 10, 16.9, 20, 30, 40, 50, 100, 200, and 1000.

ferromagnetic spin state being the ground-state solution. Away from this point at $U/t=1000$, the ferromagnetic $S=2$ ground state persists, with the magnitude of the energy difference between the lowest energy $S=0$ and $S=2$ spin states, again, being 0.12. The freezing of the energetics at $\Phi/\Phi_o = \pm 0.5$ is therefore related to the removal of Hubbard U effects in the fully polarized (ferromagnetic) state—in this case, no double occupancy and, hence, no Hubbard U contribution can occur. The onset of effective rigid rotation and near-perfect fractional periodicity corresponds to a system where the spins are well localized. Thus, the local moments for the $S=2$ ferromagnetic spin state at $\Phi/\Phi_o = \pm 0.5$ reach the maximum value of $\langle S_i^2 \rangle = 0.375$. At $U/t=40.2$, the local moment results are 0.3748 for $\Phi/\Phi_o=0$ and $\Phi/\Phi_o=\pm 0.25$. These results are close to the maximum value of $\langle S_i^2 \rangle = 0.375$. At $U/t \geqslant 40.2$, the system continues to evolve as a function of U/t for all states other than $\Phi/\Phi_o=\pm 0.5$. Figure 4 summarizes the local moment results for the t-t'-U system at $\Phi/\Phi_o=0.5$ for the $t'/t=0$ (Hubbard) and $t'/t=-0.05$ cases. The ferromagnetic transition for the $t'/t=-0.05$ system is indicated by a change in spin state to the fully polarized $S=2$ state, together with a corresponding jump in the local moment to the maximum value of 0.375. Compared to this result, the $t'/t=0$ (Hubbard) solutions show a smooth evolution of the $\Phi/\Phi_o=0.5$ state with respect to the local moment solutions and no change in the $S=0$ spin state of the system.

Figure 5 shows how the effective rigid-rotator feature of the t-t'-U system evolves as a function of t'/t. Increasing the magnitude of t'/t to 0.1 decreases the effective rigid rotation value of U/t to $U/t \sim 16.9$. The onset of effective rigid rotation again corresponds to a ferromagnetic transition to the fully polarized ($S=2$) state and freezing of the energetics in the $\Phi/\Phi_o=\pm 0.5$ results. Consequently, the local moment solutions at $\Phi/\Phi_o=\pm 0.5$ with $U/t=16.9$ have maximum values of 0.375, with local moment results for the $\Phi/\Phi_o=0$ and ± 0.25 solutions being 0.3741 in these cases.

In general, calculations for the t-t'-U system as a function of t'/t reveal an inverse relation between t'/t and U/t with respect to the onset of near-perfect fractional periodicity and effective rigid rotation. Table I shows the point of onset of an effective rigid rotation as a function of t'/t and U/t. Note that this onset also corresponds to the ferromagnetic $S=0 \to 2$ transition in the $\Phi/\Phi_o=0.5$ result. The inverse relation between the t'/t and U/t parameters seen in Table I and corresponding ferromagnetic transition are in accordance with the known properties of the quarter-filled t-t'-U chain—namely that the critical parameter setting for ferromagnetism occurs when $U \sim |t'|^{-1}$ (see Ref. 12).

The $\Delta E_{\max}$ values in Table I are defined as the maximum energy difference between the minima of the parabolas at $\Phi/\Phi_o=0$, 0.25, and 0.5. At low values of t'/t, the corresponding $\Delta E_{\max}$ values are small, which means that the system has near-perfect fractional periodicity. At $t'/t=-0.05$ and -0.1, for example, the values for $\Delta E_{\max}$ are 0.001 and 0.003, respectively. The relative closeness in energy in these solutions can be explained by a minimum Hubbard U contribution to the ground-state results occurring at $\Phi/\Phi_o=0$, 0.25 and 0.5. An inspection of the highest weighted basis states in the ground-state wave functions shows that at the point of effective rigid rotation, there are no double occupancies and, hence, no significant Hubbard U contribution to the ground-state results. Increasing $|t'/t|$ adds additional t'/t kinetics, thereby causing an increase in $\Delta E_{\max}$. This is also

TABLE I. Parameter values corresponding to the onset of effective rigid rotation, t'/t and U/t, together with $\Delta E_{\max}$ and the local moment results $\langle S_i^2 \rangle$ for the eight-site quarter-filled t-t'-U system. The first result is for the Hubbard model ($t'=0$). For $t' \neq 0$, the U/t values also indicate the point of transition to the ferromagnetic $S=2$ state, which occurs at $\Phi/\Phi_o=0.5$.

t'/t	$\sim U/t$	$\Delta E_{\max}$	$\langle S_i^2 \rangle_{\Phi/\Phi_o=0}$	$\langle S_i^2 \rangle_{\Phi/\Phi_o=0.25}$	$\langle S_i^2 \rangle_{\Phi/\Phi_o=0.5}$
0	1000	0.004	0.3750	0.3750	0.3750
−0.05	40.2	0.001	0.3748	0.3748	0.3750
−0.1	16.9	0.003	0.3741	0.3741	0.3750
−0.2	5.3	0.020	0.3701	0.3701	0.3750
−0.5	3.0	0.076	0.3671	0.3681	0.3750

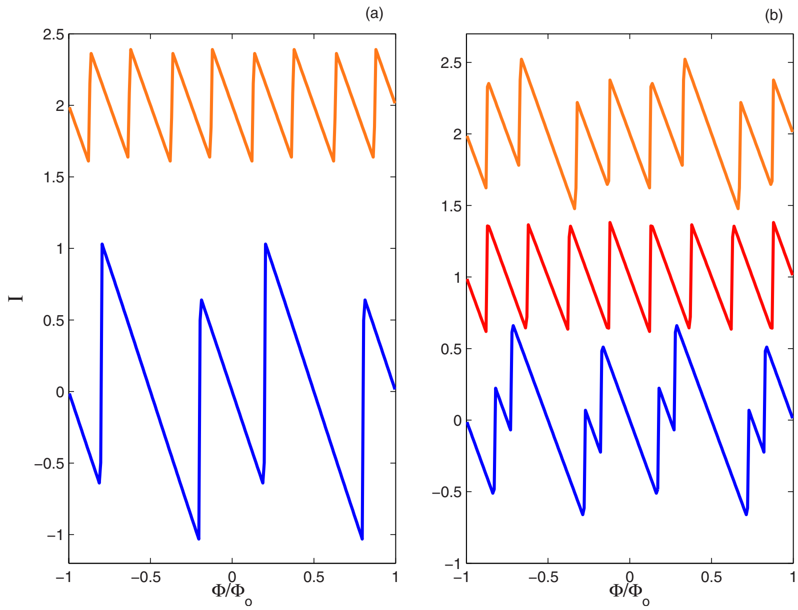

FIG. 6. (Color online) Persistent current as a function of flux, for the eight-site, quarter-filled (a) Hubbard chain with $U/t=20$ and 1000 and (b) t-t'-U system at $t'/t=-0.05$ and $U/t=20$, 40.2, and 1000, respectively. Note that the $I=0$ axis has been shifted in order to separate the results for comparison purposes.

reflected in Table I in the corresponding reduction in the local moment results.

In summary, effective rigid rotation in the t-t'-U ring can be defined by the following three criteria: (1) The first is a near-perfect Φ_o/N_e fractional periodicity, with energy minima occurring at values of $\Phi/\Phi_o=M/N_e$. These features are characterized by the relative closeness in the energy minima of the parabolas as defined by $\Delta E_{\max}$ and can be accounted for by the freezing out of the U/t energetics at $\Phi/\Phi_o=\pm 0.5$, together with a minimum Hubbard U contribution at other $\Phi/\Phi_o=M/N_e$ values. (2) The second is an $S=0\rightarrow 2$ ferromagnetic transition, which occurs at $\Phi/\Phi_o=\pm 0.5$. (3) The third maximum or near-maximum values in the local moments determined at these points.

The following trends can also be seen in the persistent current results. A comparison of the persistent current for the Hubbard [Fig. 6(a)] and t-t'-U [Fig. 6(b)] systems shows an increase in the number of peaks found in the $I(\Phi)$ curve. In particular, the $U/t=20$, t-t'-U solution shows double the number of peaks compared to the Hubbard solution. An early onset of effective rigid rotation is also evident, and this is characterized by equal amplitude peaks in the $I(\Phi)$ function. Of significance are the similarities in the results for the Hubbard system at $U/t=1000$ [Fig. 6(a)] and the t-t'-U system at $U/t=40.2$ [Fig. 6(b)]—both showing an effective rigid rotation. A characteristic of the t-t'-U system is that it undergoes a ferromagnetic transition, leading to the freezing of the energetics at $\Phi/\Phi_o=\pm 0.5$. In addition, at $\Phi/\Phi_o\neq\pm 0.5$, the energetics continue to evolve beyond the point of effective rigid rotation. This leads to a distinctive feature in the persistent current curve, namely, in the formation of signal "clusters" consisting of the same number of peaks as there are particles in the system. An example of such a cluster is shown in Fig. 6(b) for $U/t=1000$ at $-0.5\leqslant\Phi/\Phi_o\leqslant 0.5$.

B. Correspondence between the flux-penetrated t-t'-U ring and few-particle two-dimensional hard-wall quantum dot

A circularly symmetric few-particle hard-wall quantum dot (QD) is an example of an extended quasi-ring-like system. Such structures can be formed in semiconductor heterostructures by etching techniques or electrical gating of the two-dimensional electron gas (2DEG). In a typical example of the $GaAs/Al_xGa_{1-x}As$ heterostructure, the trapped electrons can be modeled as two-dimensional droplets of charges with renormalized mass $m^*=0.067m_e$ and dielectric constant $\epsilon=12.7\epsilon_0$.

A conventional choice for a model Hamiltonian for this system is

$$H=\sum_{i=1}^{N}\left[\frac{(\mathbf{p}_i+e\mathbf{A})^2}{2m^*}+V(r_i)\right]+\frac{e^2}{4\pi\epsilon}\sum_{i<j}\frac{C}{r_{ij}}, \qquad (6)$$

where $V(r)$ is the external confinement potential. In the low-density regime and at high magnetic field, the interactions between the charges are significant. While a realistic interaction potential is much softer due to screening effects, a long-range Coulomb interaction whose strength is parametrized by the dimensionless scaling factor C will be assumed. Additionally, a homogeneous external magnetic field $\mathbf{B}=\nabla\times\mathbf{A}$, perpendicular to the 2DEG plane will be included. The confinement potential is taken to be of the form

$$V(r)=0,\quad r\leqslant R=\infty,\quad r>R, \qquad (7)$$

where $R=5a_0^*$ is the radius of the dot and a_0^* is the effective Bohr radius. The choice of the hard-wall potential is motivated by the aim of having extended ring-shaped electronic structures with ferromagnetic ground-state solutions. This potential has been used in Ref. 16 to study the effect of confinement on the magneto-optical spectrum of a QD and in Refs. 17 and 18 to study the electronic structure of a QD in a strong magnetic field using a mean-field density-functional method. The most common choice of potential for quantum dots, the parabolic potential, is not a feasible choice as the ground states are not ring shaped in the regime of interest. In addition, the ground states are not ferromagnetic without a strong Zeeman term despite the effects of Landau level mixing.[20] This can be seen, e.g., in Ref. 19, which shows

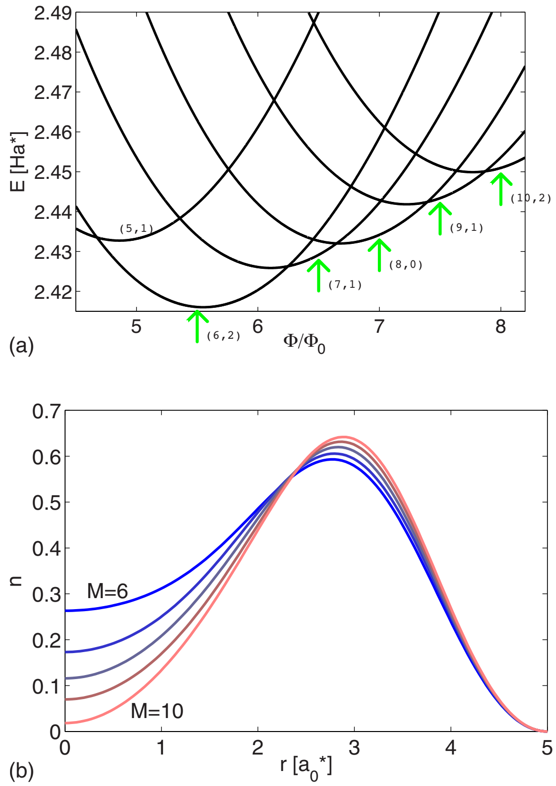

FIG. 7. (Color online) (a) Ground-state energies and (b) radial electron densities for the four-particle hard-wall quantum dot, with $M=6,\ldots,10$. The quantum numbers of the levels are shown in (a) as the pair (M,S). The cyclotron energy, $\hbar\omega_c/2$, of the zero-point motion has been subtracted from these graphs.

exact diagonalization results for electrons in a parabolic confinement, treated in the lowest-Landau-level approximation. The Zeeman coupling is therefore neglected in this work to better elucidate the interesting fact that the spin-polarized solutions are caused by the electron-electron interaction and not by the Zeeman term.

The ground-state properties of the QD system are determined numerically by diagonalizing the Hamiltonian in Eq. (6) in a basis of spin-dependent Fock states[21] built from a truncated set of lowest-lying single-particle eigenstates of the system.[16] The z component of the spin S_z and the angular momentum M are found to be good quantum numbers for this basis. The functional form of the energy eigenstates can be obtained analytically;[16] however, this has explicit dependence on the respective energy eigenvalue, which has to be solved numerically. The matrix elements of the Coulomb interactions for pairs of single-particle states are also evaluated numerically.

Figure 7 shows the ground-state energy results and the radial electron densities obtained from the eigensolutions of Eq. (6), with corresponding (M,S) values. In Fig. 7(a), the angular momentum of the ground-state energy solutions can be seen to increase as a function of the increasing total flux, $\Phi=\pi|\mathbf{B}|R^2$, in the dot. The electron density distribution [Fig. 7(b)] assumes a quasiringlike behavior, with the maximum density occurring near the mid radius. As the flux through the dot and, hence, the angular momentum is increased, the electron distribution forms a tighter ringlike structure. For example, at $M=10$, the radial electron density tends to zero at $r=0$ and at the edge of the dot at $r=5a_0$.

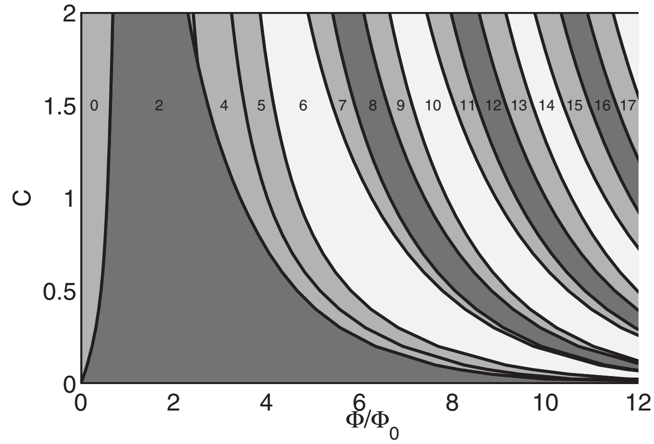

FIG. 8. Ground-state phase diagram of a four-particle hard-wall quantum dot with $R=5a_0^*$ as a function of the external magnetic flux Φ and effective interaction strength C. The shade of the filling represents the spin quantum number from dark to light $S=0,1,2$, and the integers represent the angular momentum M of the state. Fractional quasiperiodicity appears at strong Φ and C.

Further evidence of the quasi-ring-like behavior can be seen in Fig. 8, which shows the ground-state phase diagram for the dot as a function of Φ and C. Fractional quasi-periodicity in the ground-state parameters occurs as a function of the flux for strong values of Φ and C. Consistent with the flux-penetrated 1D Hubbard ring, the ground-state total spin varies periodically, with the angular momentum increasing in minimal steps of one. The spin-polarized ground states appear in angular momentum steps of N_e, which is similar to parabolic QDs in the regime of small electron numbers.[22]

Interestingly, the total spin oscillation as a function of M for the hard-wall QD (Fig. 8) is not the same as that reported by Koskinen *et al.* for the quasi-one-dimensional rings[5]—the latter system corresponds to the flux-penetrated antiferromagnetic Heisenberg model, whereas the hard-wall QD corresponds to the flux-penetrated ferromagnetic Heisenberg model. An important question then arises as to what the microscopic mechanisms for these differences between the 1D ring and the hard-wall 2D systems are.

In order to address this question, the continuum model solutions as a function of M and S are compared to those from the t-t'-U lattice model, considered to be the minimal itinerant model for ferromagnetism in 1D systems. For convenience, the continuum model results are chosen at the flux values shown by the arrows in Fig. 7(a). Since the lattice basis is not complete in the continuum description, a direct comparison is not possible. Instead, the many-body wave function $\Psi(\mathbf{x}_1,\ldots,\mathbf{x}_N)$ is projected onto a tensor-product basis of delta functions,

$$|j,\sigma_z\rangle = \delta(\mathbf{x}-\mathbf{x}_j^*)\,\delta_{\sigma,\sigma_z}, \tag{8}$$

representative of the lattice basis, with the resulting Fock expansion normalized to unity. Here, the lattice index j runs over the lattice sites, and $\mathbf{x}_j^*$ is the real-space coordinate corresponding to the jth site. The choice of $\mathbf{x}_j^*$ is not unique, as the only constraint is that the sites should form a ringlike lattice. To obtain a unique lattice, the radius is chosen to maximize the amplitude of the many-body wave function with its arguments assuming a regular polygonal configuration. Once the wave function is expressed in the lattice basis, the overlap between the continuum and corresponding lattice eigenstate solutions, $\langle\Psi_{\text{cont}}|\Psi_{\text{lattice}}\rangle$, can then be calculated.

One of the important aspects of this work is to understand the role of the electronic itineracy with respect to the magnetism seen in the continuum model results. To determine the relationship between these properties, the N_e particle continuum model solutions have been projected onto a discrete quarter-filled lattice model, having $(2N_e)$ lattice sites. To justify this choice of lattice, a specific example is given of the four-particle continuum model results projected onto an eight-site, quarter-filled lattice. Here, the maximum density droplet (MDD) state is considered, which refers to the lowest angular momentum state of the QD when the electrons are in the lowest Landau level.[23] The angular momentum of the MDD state is defined as $M_{\text{MDD}}=N_e(N_e-1)/2$. For the $N_e=4$ particle QD system, $M_{\text{MDD}}=6$. An inspection of the normalized ground-state set of eigenvector coefficients determined from the continuum model projection onto the discrete lattice demonstrates that the most highly weighted basis states for the $M_{\text{MDD}}=6$ ground state are those which are of Heisenberg type. For the quarter-filled, eight-site chain with $S_z=0$, these highly weighted states correspond to those of types $(\uparrow 0 \downarrow 0 \uparrow 0 \downarrow 0)$ and $(\uparrow 0 \uparrow 0 \downarrow 0 \downarrow 0)$, with perturbations thereof. There are 12 states of this types within the Hilbert space, which consists of a total of 784 basis states. For the normalized wave function, the corresponding weightings for each of these states is equal to 0.018. The second highest weightings are associated with basis states of types $(\uparrow \uparrow 0 \downarrow 0 \downarrow 0\ 0)$ and $(\uparrow \downarrow 0 \uparrow 0 \downarrow 0\ 0)$, together with perturbations of these, adding up to 96 basis states in total. These states have associated weightings of 0.005 each. Note specifically that the second highest weighted states have nearest-neighbor spins. This justifies the use of the extended quarter-filled lattice and brings to question the role of the kinetics with respect to the ferromagnetism seen in the continuum model result.

To determine the correspondence between the t-t'-U model and continuum model ground-state wave functions, the overlaps, $\langle\Psi_{\text{cont}}|\Psi_{\text{lattice}}\rangle$, have been calculated. Both the four-particle, $S_z=0$, and five-particle, $S_z=1/2$, continuum model cases have been considered. These cases were compared to quarter-filled eight- and ten-site t-$t'-U$ systems, respectively. The results for the maximum overlaps between the continuum and lattice model results are shown in Tables II and III. Here, the $(\Phi/\Phi_0)_{\text{cont}}$ values denote the total amount of magnetic flux that penetrates the dot. For the four-particle case, these values correspond to the flux values indicated in Fig. 7(a). A similar choice of flux values was made for the five-particle system. The maximum overlaps were determined for the first period in M, commencing at the MDD states, $M_{\text{MDD}}=6$ and $M_{\text{MDD}}=10$, for the four- and five-particle systems, respectively. The results were obtained by a careful scanning through the U/t and t'/t parameter ranges.

TABLE II. Overlap results between the eight-site quarter-filled t-t'-U ring and four-particle continuum model system. The lattice model parameters are $U/t=23$ and $t'/t=-0.17$.

L_{cont}	$(\Phi/\Phi_0)_{\text{cont}}$	$(\Phi/\Phi_0)_{\text{lattice}}$	% Overlap
6	5.5	1.5	98.4
7	6.5	1.75	98.2
8	7.0	2.0	97.8
9	7.5	2.25	97.5
10	8.0	2.5	97.1

Maximum overlaps as a function of M for the four-particle system were found to occur at $U/t=23$ and $t'/t=-0.17$ and for the five-particle system at $U/t=13$ and $t'/t=-0.19$. The dominant difference in these results lies in the strength of the Hubbard U. A larger U/t value for the four-particle system is consistent with what is known in the continuum model description of quantum rings, namely, that these systems become more interaction dominated when they contain fewer particles. Given the similar magnitude of t'/t in the four-particle and five-particle cases, it seems apparent that the role of this parameter is therefore to simulate the correct extended geometry of the ring. As M is increased, the continuum model systems become more ringlike, losing some of these extended system qualities. Thus, for larger M, the maximum overlaps for both the four- and five-particle cases are found to slightly decrease.

In Figs. 9 and 10, the ground-state energy results as a function of flux for the eight-site and ten-site t-t'-U ring systems are shown with the choice of t'/t values being the same as those which were required to achieve a maximum overlap. The values of U/t required for a maximum overlap occur after the point of effective rigid rotation in both of these cases. From the lattice model perspective, this result shows that the system has undergone the ferromagnetic transition required to initiate an effective rigid rotation. The total spin progression for both the continuum and lattice model systems as a function of M therefore follows that of the flux-penetrated ferromagnetic Heisenberg model,

TABLE III. Overlap results between the ten-site quarter-filled t-t'-U ring and five-particle continuum model system. The lattice model parameters are $U/t=13$ and $t'/t=-0.19$.

L_{cont}	$(\Phi/\Phi_0)_{\text{cont}}$	$(\Phi/\Phi_0)_{\text{lattice}}$	% Overlap
10	6.9	2.0	98.5
11	7.3	2.2	98.1
12	7.7	2.4	97.8
13	8.1	2.6	97.7
14	8.5	2.8	97.6
15	8.8	3.0	97.4

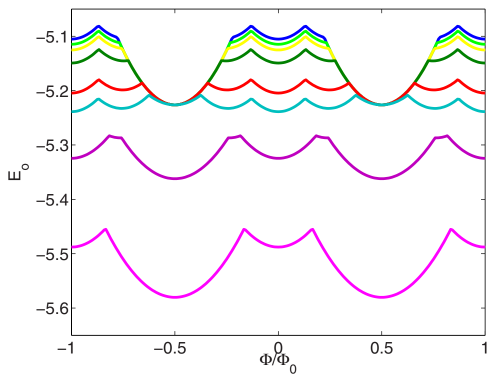

FIG. 9. (Color online) Ground-state energy as a function of flux for an eight-site, quarter-filled t-t'-U chain with $t'/t=-0.17$. The values of U/t starting from the bottom curve are 3, 5, 7.28, 10, 23, 50, 100, and 1000. Note that the point of effective rigid rotation occurs at $\simeq U/t=7.28$.

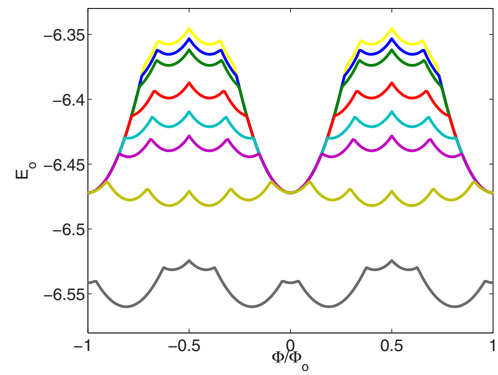

FIG. 10. (Color online) Ground-state energy as a function of flux for the ten-site, quarter-filled t-t'-U chain with $t'/t=-0.19$. The values of U/t starting from the bottom curve are 5, 6.47, 10, 13, 20, 50, 100, and 1000. Note that the point of effective rigid rotation occurs at $\simeq U/t=6.47$.

namely, $(M,S)_4=(6,2)\rightarrow(7,1)\rightarrow(8,0)\rightarrow(9,1)\rightarrow(10,2)$ and $(M,S)_5=(10,\frac{5}{2})\rightarrow(11,\frac{3}{2})\rightarrow(12,\frac{1}{2})\rightarrow(13,\frac{1}{2})\rightarrow(14,\frac{3}{2})\rightarrow(15,\frac{5}{2})$, for the four-particle and five-particle cases. The high correspondence between the continuum and lattice model systems, which is between 97% and 98%, demonstrates clearly that, similar to the t-t'-U system, the additional degree of kinetic freedom and extended ringlike geometry are the important factors that are responsible for the ferromagnetism seen in the continuum model results.

In summary, to encapsulate the correct physics and the kinetics in the continuum QD system, the t-t'-U lattice needs to be double in size and, hence, quarter filled with respect to the total particle number. To obtain a maximum overlap, the lattice model needs to have evolved beyond the point of rigid rotation, which is denoted by the onset of a ferromagnetic phase, thus corresponding to the ferromagnetism seen in the continuum model results.

IV. CONCLUSION

The flux-penetrated t-t'-U 1D system at quarter filling has been investigated as a function of t'/t and U/t parametrization. The results indicate an onset of effective rigid rotation in this system, which occurs for moderate U/t values, and coincides with a ferromagnetic transition. This model has been used to explain the essential physics of the continuum model results for a few-particle 2D quantum dot. For four- and five-particle cases, the maximum overlaps between the continuum and lattice model wave functions give 97%–98% correspondence. The ferromagnetism, which is seen in the continuum model solutions, can be explained by the additional kinetics and extended ringlike geometry. The results suggest the possibility of antiferromagnetic to ferromagnetic switching from strictly 1D to extended quantum ring systems. In addition, a decrease in the order of magnitude of the Hilbert space size in the lattice model compared to the continuum model indicates that the lattice model may be a more efficient method of determining the ground-state properties and essential physics of extended ring QD systems.

ACKNOWLEDGMENT

This work was supported by the Academy of Finland through its Centre of Excellence Program (2000–2011).

*yvh@fyslab.hut.fi

[1] S. M. Reimann and M. Manninen, Rev. Mod. Phys. **74**, 1283 (2002).
[2] A. Lorke, R. J. Luyken, A. O. Govorov, J. P. Kotthaus, J. M. Garcia, and P. M. Petroff, Phys. Rev. Lett. **84**, 2223 (2000).
[3] U. F. Keyser, C. Fühner, S. Borck, R. J. Haug, M. Bichler, G. Abstreiter, and W. Wegscheider, Phys. Rev. Lett. **90**, 196601 (2003).
[4] J. Hubbard, Proc. R. Soc. London, Ser. A **276**, 238 (1963).
[5] M. Koskinen, M. Manninen, B. Mottelson, and S. M. Reimann, Phys. Rev. B **63**, 205323 (2001).
[6] S. Viefers, P. Koskinen, P. Singha Deo, and M. Manninen, Physica E (Amsterdam) **21**, 1 (2004).
[7] N. Yu and M. Fowler, Phys. Rev. B **45**, 11795 (1992).
[8] F. V. Kusmartsev, J. Phys.: Condens. Matter **3**, 3199 (1991).
[9] F. V. Kusmartsev, J. F. Weisz, R. Kishore, and M. Takahashi, Phys. Rev. B **49**, 16234 (1994).
[10] F. V. Kusmartsev, Phys. Rev. B **52**, 14445 (1995).
[11] K. Niemelä, P. Pietiläinen, P. Hyvönen, and T. Chakraborty, Europhys. Lett. **36**, 533 (1996).
[12] S. Daul and R. M. Noack, Phys. Rev. B **58**, 2635 (1998).
[13] E. H. Lieb and D. Mattis, Phys. Rev. **125**, 164 (1962).
[14] S. K. Maiti, J. Chowdhury, and S. N. Karmaker, J. Phys.: Condens. Matter **18**, 5349 (2006).
[15] http://www.caam.rice.edu/software/ARPACK/
[16] F. Geerinckx, F. M. Peeters, and J. T. Devreese, J. Appl. Phys. **68**, 3435 (1990).
[17] E. Räsänen, A. Harju, M. J. Puska, and R. M. Nieminen, Phys.

Rev. B **69**, 165309 (2004).
[18] E. Räsänen, H. Saarikoski, Y. Yu, A. Harju, M. J. Puska, and S. M. Reimann, Phys. Rev. B **73**, 235324 (2006).
[19] M. Koskinen, S. M. Reimann, J.-P. Nikkarila, and M. Manninen, J. Phys.: Condens. Matter **19**, 076211 (2007).
[20] S. Siljamäki, A. Harju, R. M. Nieminen, V. A. Sverdlov, and P. Hyvönen, Phys. Rev. B **65**, 121306(R) (2002).
[21] S. S. Gylfadóttir, A. Harju, T. Jouttenus, and C. Webb, New J. Phys. **8**, 211 (2006).
[22] H. Saarikoski and A. Harju, Phys. Rev. Lett. **94**, 246803 (2005).
[23] A. H. MacDonald, S. R. Eric Yang, and M. D. Johnson, Aust. J. Phys. **46**, 345 (1993).